# Quadratic Phase Coding for High Duty Cycle Radar Operation

JAMES B. MEAD AND ANDREW L. PAZMANY

*ProSensing, Inc., Amherst, Massachusetts*

(Manuscript received 5 July 2018, in final form 18 March 2019)

ABSTRACT

Quadratically varying phase codes applied from pulse to pulse can be used to impart a range-dependent frequency shift in the decoded signal of a pulsed radar. Radars employing such codes can operate at extremely high pulse repetition frequencies (PRFs) with overlaid signals from multiple echo trips separated in the spectral domain. When operating at high PRFs, the radar duty cycle can approach 50% in a single-antenna system. High duty cycle operation results in a substantial increase in average transmit power with a proportional increase in signal processing gain as compared to a conventional pulsed radar. The shortest quadratic phase code, or base code, has a length equal to the number of echo trips $M$ that can be unambiguously resolved in the spectral domain. The decoded waveform is essentially free from range sidelobes under ideal conditions. However, amplitude and phase errors associated with nonideal phase coding result in range sidelobes that appear at all echo trips in the decoded signal. These sidelobes can be suppressed by using a composite phase code composed of a periodically repeating base phase code added to a much longer quadratic code with a proportionally slower phase variation. Meteorological data gathered with a Ka-band radar operating at 3.0-MHz PRF at 45% duty cycle are presented. A comparison of these data with data gathered in short-pulse mode at a duty cycle of 0.3% exhibited a 21-dB improvement in the Doppler spectrum signal-to-noise ratio, equal to the ratio of the respective duty cycles.

## 1. Introduction

This paper describes the use of quadratically varying phase codes in pulsed radar to separate overlaid signals from multiple echo trips in the spectral domain. This technique, termed quadratic phase coded (QPC) radar, allows operation at high pulse repetition frequencies (PRFs), several orders of magnitude higher than would be used by a conventional pulsed radar. The sampled QPC radar signal is processed using a discrete Fourier transform (DFT) to generate the Doppler spectrum. It has been shown that optimal DFT-based signal processing gain is linearly proportional to the PRF (Mead 2016). Therefore, the high PRFs associated with QPC radar operation can yield several orders of magnitude improvement in postprocessed signal-to-noise ratio (SNR) relative to a conventional pulsed radar having the same range resolution.

A comparison of achievable SNR between QPC radar and other radar techniques is most readily understood in terms of transmitter duty cycle. For radars observing pulse volumes with coherence times much greater than the pulse repetition time, such as surveillance or weather radars, the postprocessed SNR[1] is linearly proportional to the average transmitted power (Raemer 1996). Therefore, for a given peak transmitter power the postprocessed SNR scales linearly with transmitter duty cycle. Duty cycle can be maximized by employing the longest practical transmitted pulse for a given PRF or by maximizing the radar PRF for a given pulse length. For pulse compression radar and frequency-modulated continuous wave (FMCW) radar (Skolnik 1990), long pulses are transmitted, with processing gain approximately equal to the time-bandwidth product of the coded waveform (Skolnik 2008). For a given range resolution, the bandwidth is fixed; therefore, sensitivity scales linearly with pulse length and therefore scales linearly with duty cycle for a given PRF.

The duty cycle achievable in a pulse compression radar is limited by the capability of the transmitter as well

Denotes content that is immediately available upon publication as open access.

*Corresponding author*: James B. Mead, mead@prosensing.com

[1] Throughout the text, signal processing assumes a matched filter receiver followed by phase coherent summation of multiple samples during the dwell time. Coherent summation is achieved through DFT processing.

DOI: 10.1175/JTECH-D-18-0108.1

© 2019 American Meteorological Society. For information regarding reuse of this content and general copyright information, consult the AMS Copyright Policy (www.ametsoc.org/PUBSReuseLicenses).

as by the minimum range set by the usual requirement that the receiver be blanked during pulse transmission. Full compression gain is achieved only for ranges $R$, such that $DR_{\max} < R < (1 - D)R_{\max}$, where $R_{\max}$ is the maximum unambiguous range and $D$ is the transmitter duty cycle. For duty cycles exceeding 25%, less than half of the maximum unambiguous range can be observed with full compression gain. Therefore, pulse compression radars typically operate with duty cycles of 25% or less. Pulse compression waveforms with high compression ratios result in high minimum ranges and are often accompanied by a short pulse transmitted after the pulse compression waveform (McLinden et al. 2013; Pazmany and Haimov 2018). This means that the near-range samples are limited in sensitivity to that of the short pulse, typically employing less than 1% of the duty cycle capability of the amplifier.

For FMCW radar, the duty cycle can approach 100%, although the duty cycle is reduced to as low as 50% when the maximum measurement range is a significant fraction of the unambiguous range (Delanoë et al. 2016). SNR in FMCW radar is often limited by AM and FM noise associated with transmitter to receiver leakage (Skolnik 1990). This leakage can be minimized by using separate antennas for the transmitter and receiver. The requirement for separate transmit and receive antennas is a significant drawback of FMCW radar because of several factors, including parallax at close ranges, the need for careful antenna to antenna alignment, and a doubling of the area required for the antenna apertures.

Sachidananda and Zrnic (SZ) phase coding (Sachidananda and Zrnic 1999), in which the discrete-time integral of a quadratically varying sequence is transmitted, is employed in NEXRAD to aid in removing multitrip echo contamination. For the SZ technique, the decoded waveform of the desired echo trip (typically the first or second trip) is unaffected, while other echo trips are modulated by the phase code. This modulation causes the undesired echo energy to be divided and distributed to a number of subregions of the power spectrum. While SZ coding has proven to be effective in recovering up to two overlaid echoes, it is not viable when many echo trips are present, since the various echo trips would overlap in the spectrum and not be separable.

QPC radar achieves the signal processing gain associated with high duty cycle operation without the penalty of large minimum range as exhibited by pulse compression radar, and without the need for separate transmit and receive antennas, as in the case of FMCW radar. When used with a single antenna, the transmitter duty cycle of a QPC radar can approach 50%, limited only by the switching speed of the transmit–receive network, as detailed in appendix A. In a dual-antenna QPC radar, the transmitter duty cycle is 100%. The ability to operate at high duty cycle is generally determined by the capability of the final transmitter amplifier. Most high-power, tube-based transmitters operate at relatively low duty cycles, on the order of 10% or less. Furthermore, high-voltage modulators required to operate these tubes are usually limited to PRFs on the order of 10–100 kHz. Therefore, tube-based transmitters designed for pulsed operation cannot achieve the high transmitter duty cycles or high PRFs required for effective QPC radar operation. By contrast, many solid-state power amplifiers (SSPAs) are available that can operate both at very high PRFs and high duty cycles. These SSPAs are ideally suited for QPC radar.

Polyphase codes with quadratically varying phase have been used extensively for communications and radar applications (Chu 1972; Lewis et al. 1986). Quadratically varying phase codes can be thought of a discrete sampling of a linear FM waveform (Lundén et al. 2005). For example, the P3 code (Lewis et al. 1986; Skolnik 2008) is of the form

$$\phi_n = \frac{\pi n^2}{\rho}, \quad n = 0, 1, 2, \ldots, \rho - 1$$

and yields a pulse compression gain equal to the code length $\rho$. Such polyphase codes, when used to set the starting phase of successive pulses, induce an echo trip–dependent frequency shift in the received signal when decoded by the complex conjugate of the transmitted code. This frequency shift allows overlaid signals from multiple echo trips to be separated in the spectral domain. The use of a quadratically varying phase code from pulse to pulse was first described in a patent by Lee (2015) with an emphasis on separating ambiguous Doppler spectra in regions of high shear in severe storms. The present paper focuses on signal processing gain achieved by high duty cycle operation with quadratic phase coding and introduces the concept of composite codes to suppress range sidelobes induced by phase and amplitude errors.

This paper is organized as follows. The QPC radar technique is described in section 2. Section 3 describes a special QPC radar operating mode termed phase-modulated square wave (PMSW), which is shown to result in the highest possible SNR for a QPC radar using a single antenna with the receiver blanked during transmission. An approximate formula for integrated range sidelobes is presented for PMSW mode, showing that range sidelobes are negligible in the absence of amplitude and phase errors. Spurious artifacts due to amplitude and phase errors in the decoded signal are described in section 4. These artifacts appear throughout the spectrum and lead to significant range sidelobes in the presence of strong

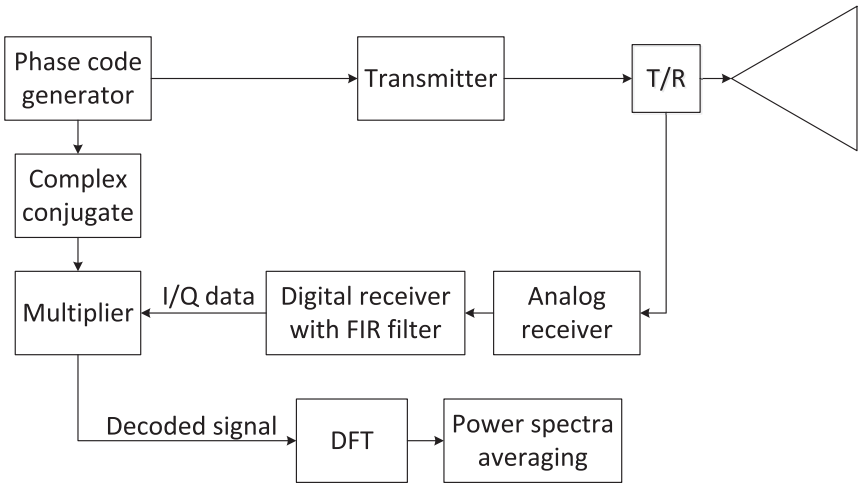


FIG. 1. QPC radar architecture.

signals. Section 5 introduces the concept of composite quadratic codes, which combine a base quadratic code with a much longer quadratic code to suppress spurious-induced range sidelobes. In the case of composite codes, the spurious artifacts are found to limit dynamic range, but for a carefully designed system the dynamic range will be on the order of 80 dB. Section 6 presents QPC radar data gathered in PMSW mode. Data presented show over 20-dB improvement in signal-to-noise ratio achieved through signal processing gain as compared to conventional short-pulse operation.

## 2. QPC radar technique

Consider a radar operating at a multiple of a base pulse repetition frequency $F_p^0$ given by

$$F_p^0 = \frac{c}{2R_{\max}}, \tag{1}$$

where $R_{\max}$ is the maximum expected target range and $c$ is the speed of light. The pulse repetition frequency is

$$F_p = MF_p^0, \tag{2}$$

where $M$ is the PRF multiplication factor. If targets exist at all ranges up to $R_{\max}$, then a PRF of $M$ times the base PRF will result in $M$ overlaid signals in each range gate. Applying a periodic quadratic phase code to the transmit waveform allows these ambiguous return signals to be separated in the frequency domain.

The base quadratic phase code is generated as follows:

$$\phi_n = n^2\phi_1, \quad n = 0, 1, 2, \ldots, L_0 - 1, \tag{3}$$

$$\phi_1 = \frac{\pi}{M}, \tag{4}$$

where $n$ is the pulse index and $L_0$ is the base-code length:

$$\begin{aligned} L_0 &= M \quad \text{for} \quad M \text{ even}, \\ L_0 &= 2M \quad \text{for} \quad M \text{ odd}. \end{aligned} \tag{5}$$

The base code is applied repeatedly, such that

$$\phi_{kL_0+n} = \phi_n, \quad k = 0, 1, 2, \ldots, \tag{6}$$

so that the phase code is periodic.

The base code is a P3 code with the pulse compression ratio equal to $M$ (Lewis and Kretschmer 1982) and is palindromic, being symmetric around $L_0/2$ when viewed modulo $2\pi$ (Lewis et al. 1986). The P3 code is inherently Doppler tolerant, although it is subject to range–Doppler coupling, as with linear FM waveforms (Lewis et al. 1986).

The QPC radar architecture is shown in Fig. 1. The phase of the transmit waveform is advanced on each pulse according to (3). Upon reception, the received waveform is digitized and downconverted to baseband by a digital receiver. The in-phase and quadrature (I/Q) signals representing the received signal's complex envelope are filtered using a low-pass finite impulse response (FIR) filter matched to the bandwidth of the pulse. This signal is multiplied by the complex conjugate of the phasor representing the initial phase of the latest transmit waveform, which subtracts the phase of the current transmit pulse from the received signal's phase.

Because of the high PRF required for QPC radar, the received signal for a particular range gate is the sum of multiple signals from different ranges. Multiple signals appearing in a single range gate are referred to as overlaid echoes. The echo trip index $m = 0, 1, 2, \ldots, M - 1$ refers

to the various overlaid echoes; for example, $m = 0$ corresponds to the first trip echo. The echo trip spacing in range is given by

$$\delta = 0.5cF_p^{-1}. \tag{7}$$

The sampled range vector is composed of $N_g$ range gates:

$$N_g = 1 + (\delta - R_0)/\Delta R_g, \tag{8}$$

where $\Delta R_g$ is the range gate spacing and $R_0$ is the range offset of the first range gate. The sampled range $R_s$ is given by

$$R_s = R_o + i\Delta R_g, \quad i = 0, 1, \ldots, N_g - 1. \tag{9}$$

The true range for a particular range gate and echo trip $R(m, i)$ is given by

$$R(m,i) = R_s + m\delta, \quad m = 0, 1, \ldots, M - 1. \tag{10}$$

The code-induced phase shift of the decoded signals from the $m$th echo trip, for which the phase is delayed by $m$ samples, is given by

$$\tilde{\phi} = \phi_{n-m} - \phi_n = \phi_1[(n-m)^2 - n^2] = \phi_1(m^2 - 2nm). \tag{11}$$

The change in phase from pulse to pulse for a signal from echo trip $m$ is

$$\frac{\Delta\tilde{\phi}}{\Delta n} = -2m\phi_1, \tag{12}$$

where the time index $n$ increments by one from pulse to pulse ($\Delta n = 1$). The discrete time derivative of the decoded phase (rad s$^{-1}$), equal to the instantaneous frequency shift of the $m$th echo trip, is given by

$$\Delta f_m = \frac{\Delta\tilde{\phi}}{\Delta n}\frac{\Delta n}{\Delta t} = -2m\phi_1 F_p = -2m\left(\frac{\pi}{M}\right)F_p. \tag{13}$$

Noting that $F_p = MF_p^0$ and dividing by $2\pi$ to convert from radians to hertz gives

$$\Delta f_m = -mF_p^0. \tag{14}$$

This equation shows that the frequency shift of the decoded signal from the $m$th echo trip is proportional to the echo index $m$ and that the frequency shift between successive echo trips is equal to the base PRF. Combining (10) and (14) shows that a linear relationship exists between the range of the $m$th echo trip and frequency shift:

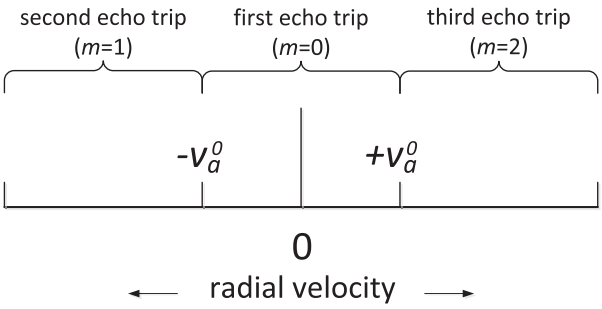


FIG. 2. Location of echo trips in the spectral domain for $M = 3$. The parameter $v_a^0 = F_p^0\lambda/4$ is the maximum unambiguous velocity associated with the base PRF.

$$\Delta f_m = \frac{R_s - R(m,i)}{\delta}F_p^0. \tag{15}$$

This linear transformation from the range domain to the frequency domain is analogous to the same process in FMCW radar (Skolnik 1990).

For each range gate, a block of samples of the decoded signal is processed using a DFT to estimate the voltage spectrum. As with conventional Doppler processing, the number of samples input to the DFT is determined by the PRF and the dwell time required to achieve the desired velocity resolution $\Delta_v$. The dwell time per DFT $T_D$, identical to that of a conventional radar, is given by

$$T_D = \lambda/(2\Delta_v), \tag{16}$$

where $\lambda$ is the radar wavelength. Multiple spectra are typically power averaged to reduce the variance of the individual spectral components (Press et al. 1988; Mead 2016). Following averaging, the power spectrum is partitioned into $M$ segments to separate the Doppler spectra associated with the various echo trips.

Consider an example where the PRF multiplication factor $M = 3$. The received signal prior to decoding for a particular range gate is composed of the complex sum of three overlaid echo trips ($m = 0, 1, 2$). The signals from the various echo trips are distributed in this range gate's spectrum as shown in Fig. 2. As with a conventional pulsed radar, the maximum unambiguous velocity $v_a^0$ corresponding to the signal for each echo trip is

$$v_a^0 = \frac{F_p^0\lambda}{4}. \tag{17}$$

If the maximum velocity $v_m^{\max}$ for a signal with echo trip index $m$ exceeds $v_a^0$ such that

$$pv_a^0 \le v_m^{\max} \le (p+1)v_a^0, \tag{18}$$

where $p$ is a positive integer, the signal will fall into the region of the spectrum corresponding to echo trip index

$$\begin{aligned} &m-p \quad \text{for} \quad p \le m, \\ &M+m-p \quad \text{for} \quad p > m. \end{aligned} \tag{19}$$

This is analogous to the range–Doppler ambiguity in FMCW radar where large Doppler shifts result in a range offset of the signal as well as Doppler aliasing.

In QPC radar operation, there are $M$ times as many pulses gathered within a given observation time as compared to the number of samples gathered with a conventional pulsed radar. Thus, when using coherent processing, such as with the DFT-based spectral estimation, the coherent gain relative to conventional pulsed radar is equal to $M$. This statement is equivalent to the fact that signal processing gain is proportional to PRF for a given dwell time provided the signal is correlated from pulse to pulse (Mead 2016).

## 3. Phase-modulated square wave radar

In appendix A, the duty cycle that optimizes SNR is shown to be 50%, assuming single-antenna operation with ideal transmit/receive (T/R) switching. Operating a QPC radar near 50% duty cycle is termed PMSW radar. To operate in PMSW mode, the PRF multiplication factor is selected such that

$$M = \frac{R_{\max}}{2\Delta R_0}, \tag{20}$$

where $\Delta R_0$ is the desired range resolution, determined by the ideal pulse width $\tau_0$ assuming a perfect T/R network with zero switching delay; that is,

$$\Delta R_0 = \frac{c\tau_0}{2} = 0.5\delta. \tag{21}$$

In practice, the T/R network has finite response time as described in appendix A. Therefore, the true range resolution will be less than $\Delta R_0$. The radar data system is configured to store a single decimated sample for each transmitted pulse; that is, $N_g = 1$ as shown in Fig. 3. The samples are decoded by multiplying with the complex conjugate of the current transmit phase then the decoded samples are processed by a single DFT to compute the Doppler spectrum at all observed ranges.

When operating in PMSW mode, the receiver is periodically blanked at a high rate to protect the receiver from transmitter leakage. Therefore, the signal is sampled at a range spacing that is slightly larger than twice the range resolution determined by the pulse length, assuming some finite T/R network switching time. This implies that the received signal has gaps that are somewhat larger than the range resolution between successive echo trips. This undersampling of the received signal leads to some loss of information as compared to a conventional pulsed radar for which, typically, $\Delta R_g \le \Delta R_0$. The gaps in the range profile may be a drawback when studying, for example, the fine structure near cloud top or bottom or very thin cloud layers.

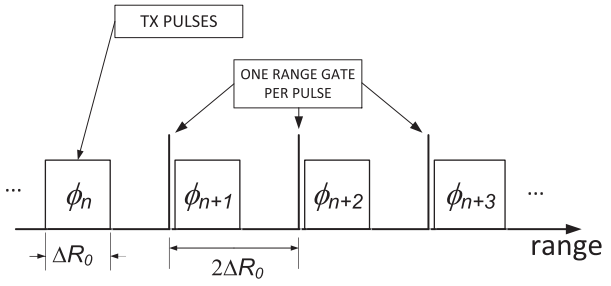


FIG. 3. PMSW mode. The transmit phase is marked in each transmit pulse. The voltage sampled at each range gate represents the complex sum of signals from all $M$ echo trips.

### *Range sidelobes in PMSW mode*

Range sidelobes in PMSW mode arise because of spectral leakage that causes signal power associated with a particular echo trip to appear in the spectral region associated with other echo trips. Spectral leakage results from the finite length of the time domain sample vector used in computing the spectrum as well as the inherent spectral broadening associated with the window function applied to the signal prior to DFT processing. For PMSW radar, a single DFT is performed to create the Doppler spectrum for all ranges. By contrast, conventional pulsed or FMCW radar requires separate DFTs to be executed at each range gate to generate the Doppler spectrum (Barrick 1973). In PMSW radar, the length of the DFT ($N$) can be determined from the desired velocity resolution:

$$N = \text{floor}\left(\frac{F_p\lambda}{2\Delta v}\right) = \text{floor}\left(\frac{MF_p^0\lambda}{2\Delta v}\right), \tag{22}$$

where the "floor" operator rounds down to the nearest integer. Thus, the DFT length scales linearly with the PRF multiplication factor to maintain constant velocity resolution.

Within the PMSW spectrum, the Doppler spectrum for the $m$th echo trip, located at range $R(m, 0)$ is composed of $\tilde{N}$ samples:

$$\tilde{N} = \text{floor}\left(\frac{N}{M}\right) = \text{floor}\left(\frac{F_P^0\lambda}{2\Delta v}\right), \tag{23}$$

with Doppler spectra for successive echo trips separated by $\tilde{N}$ spectral components. Integrated sidelobe

power for a point target from the $m$th echo trip is found by summing the total sidelobe power over the entire spectrum excluding the region of the spectrum associated with this echo trip and comparing the summed power to the peak signal power. Integrated sidelobe power, assuming ideal phase coding, is plotted in Fig. 4, along with an empirically determined approximate formula, assuming that a Hanning window is applied to the time domain signal:

$$\mathrm{SLL\,(dB)} \approx 3 - 51.5\log_{10}(\tilde{N}) + 46\left(\frac{v_0}{v_a^0}\right)^2,$$
$$0 < v_0 < 0.8v_a^0, \tag{24}$$

where $v_0$ is the mean signal velocity. For example, $\tilde{N} = 215$ for a desired velocity resolution of 20 cm s$^{-1}$ for a Ka-band radar ($\lambda = 0.0086$ m) with a base PRF of 10 kHz. In this case, the integrated sidelobe level ranges from $-117$ dBc for $v_0 = 0$ to $-88$ dBc for $v_0 = 0.8v_a^0$. Over 99.8% of the integrated sidelobe power for a signal associated with echo trip $m$ is contained in the neighboring echo trips $m - 1$ and $m + 1$.

## 4. Effects of phase and amplitude errors in PMSW mode

Phase and amplitude errors introduced by distortions in the transmitter and receiver cause spurious signals in the decoded spectrum. These errors can arise from various sources, including quantization errors, distortions in the radar's analog circuitry, and the transfer function of the digital receiver and its associated FIR filter. The spurious signals are spread throughout the spectrum and therefore appear as range sidelobes that are present at all observed ranges. In a QPC radar system, the instantaneous phase error $\varepsilon$ and normalized amplitude error $\alpha$ are found to be a function of the current transmit phase such that $\varepsilon = f(\phi_n)$ and $\alpha = g(\phi_n)$. Since the phase code is periodic with period $L_0$, the amplitude and phase errors are also periodic with period $L_0$. Assuming small RMS amplitude and phase errors, $\sigma_\alpha$ and $\sigma_\varepsilon < 0.1$, the expected value of the spurious power associated with a scattering volume at a particular range location is $(\sigma_\alpha^2 + \sigma_\varepsilon^2)P_m$, where $P_m$ is the average power in the $m$th echo trip. This result is derived in appendix B. Total spurious power $P_s^T$ is given by

$$P_s^T = (\sigma_\alpha^2 + \sigma_\varepsilon^2)\Sigma_P, \tag{25}$$

where $\Sigma_P$ represents the total signal power over all echo trips:

$$\Sigma_P = \sum_{m=0}^{M-1} P_m. \tag{26}$$

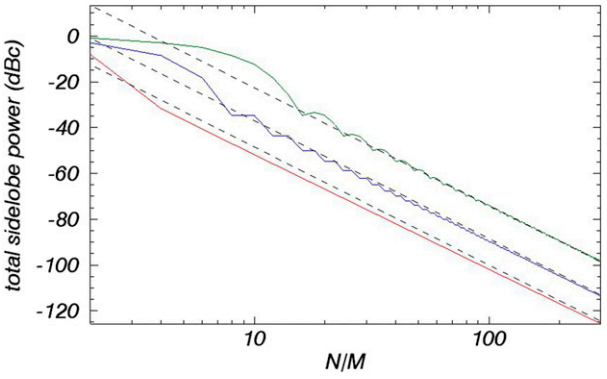


FIG. 4. Total sidelobe power relative to peak spectral power as a function of the number of velocity bins per echo trip $\tilde{N} = N/M$: $v_0 = 0$ (red), $v_0 = 0.5v_a^0$ (blue), and $v_0 = 0.75v_a^0$ (green). The approximate formula, (24), is shown with dashed lines.

Since $\alpha$ and $\varepsilon$ are periodic with period $L_0$, the resultant spurious for each echo trip has a Fourier series representation with spurious signal coefficients spaced at $\Delta f_s$:

$$\Delta f_s = \frac{F_p}{L_0} = \frac{MF_p^0}{L_0}. \tag{27}$$

For odd length codes, $L_0 = 2M$; thus, spurs occur at a spacing of $\Delta f_s = 0.5F_p^0$. For even length codes, $\Delta f_s = F_p^0$.

An interactive data language (IDL) program was written to simulate the power spectrum of the return signal from a QPC radar operating in PMSW mode. Simulated weather signals with a given spectral width were generated using the method described in Sirmans and Bumgarner (1975). Deterministic amplitude and phase errors were computed as a function of the transmitted phase. The functional dependence of these errors was found using the radar described in section 6 by feeding the attenuated Ka-band output of the transmitter back into the receiver. A simulated spectrum for a point target located within the first echo trip is plotted in Fig. 5 using a phase code with $M = 500$. The base PRF was set to 10 kHz, so that $F_p = 5$ MHz, and the error standard deviations were set to $\sigma_\alpha = \sigma_\varepsilon = 0.01$. The average spurious level of $-64.0$ dBc was found using (25) to find the total spurious power then dividing by the number of spurs, equal to $M - 1$. The central 100 kHz of the spectrum shown in Fig. 5 is plotted in Fig. 6 showing spurious signals spaced at $F_p^0$. The spurious signals appear as range sidelobes that track the signal velocity. These range sidelobes will generally span the full range interval 0–$R_{\max}$.

## 5. Composite phase codes in PMSW mode

To suppress spurious-induced range sidelobes, a phase code can be created from the composite of a periodically

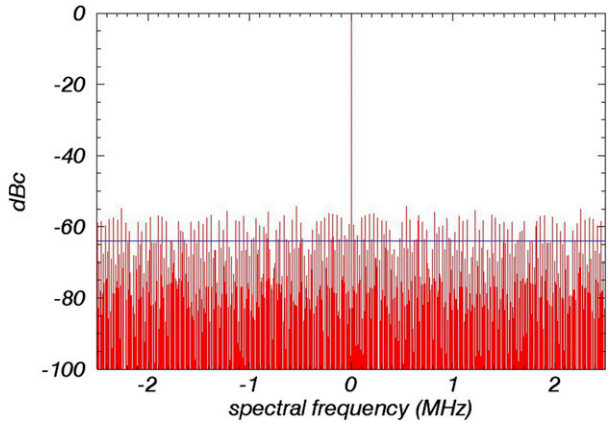


FIG. 5. Simulated spectrum with $M = 500$, $\sigma_\varepsilon = 0.01$, and $\sigma_\alpha = 0.01$. Theoretical average spurious of −64.0 dBc is shown with the solid blue line.

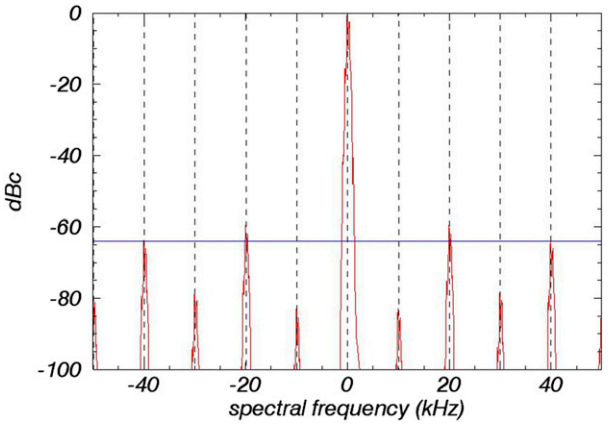


FIG. 6. As in Fig. 5, but showing detail near spectral peak at zero frequency. Center frequency for the various echo indices is shown with dashed lines with $m = 0$ at 0 Hz, $m = 1$ at −10 kHz, $m = 2$ at −20 kHz, ..., and $m = M - 1$ at 10 kHz. The spurious falling on the vertical dashed lines appears as range sidelobes that track the velocity of the signal. Theoretical average spurious of −64.0 dBc is shown with the solid blue line.

repeating base code given by (3) with a much longer P3 code having a proportionally smaller value of the phase increment. The composite code is given by

$$\begin{aligned} \phi_n &= n^2\phi_c, \quad n = 0, 1, 2, \ldots, L_c - 1, \\ \phi_c &= \phi_1 + \phi_p, \end{aligned} \tag{28}$$

where $L_c$ is the composite code length ($L_c = \Gamma L_0$, where $\Gamma$ is an integer $\gg 1$) and $\phi_c$ is the composite code phase increment. The perturbation phase increment, $\phi_p$ is

$$\phi_p = \frac{2\pi}{L_c}. \tag{29}$$

As with the base code (3), the composite code is applied periodically. The base phase code, determined by the $\phi_1$ term in (28), is periodic with period $L_0$ when viewed modulo $2\pi$. When $\phi_p$ is computed using (29) for a large value of $L_c$, the composite code in (28) slowly diverges from the base code, which means that the spectrum of the demodulated waveform is very similar to that found when using the base code, with the frequency associated with the center of each echo trip shifted slightly more in the Doppler domain than with the base code:

$$\begin{aligned} \Delta f_m &= \frac{\Delta\tilde{\phi}}{\Delta n}\frac{\Delta n}{\Delta t} = -2m(\phi_1 + \phi_p)F_p \text{ rad s}^{-1} \\ &= -mF_p^0\left(1 + \frac{2}{\Gamma K}\right) \text{Hz}, \quad \text{with} \\ K &= 1 \text{ when } M \text{ is even and } K = 2 \text{ when } M \text{ is odd}. \end{aligned} \tag{30}$$

The additional frequency shift induced by the perturbation phase increment reduces the number of echo trips that fit within the decoded signal spectrum without aliasing. This value, termed $m_{\max}$, is found by taking the ratio of the frequency shift associated with the base code (13) to that of the composite code (30) and multiplying by $M$, the number of echo trips associated with the base code:

$$m_{\max} = \text{floor}\left(\frac{\Gamma KM}{2 + \Gamma K}\right). \tag{31}$$

The floor function is applied to yield an integer number of echo trips. For long composite codes ($\Gamma K > 100$), $m_{\max}$ is within 2% of $M$. If the multiplied PRF is left unchanged as compared to that obtained with the base code, then the base PRF assumes a somewhat higher effective value $\tilde{F}_p^0$ found by scaling $F_p^0$ by the ratio $M/m_{\max}$:

$$\tilde{F}_p^0 = F_p^0\frac{(2 + \Gamma K)}{\Gamma K}, \tag{32}$$

which slightly increases the maximum unambiguous velocity:

$$v_a^0 = \frac{\tilde{F}_p^0\lambda}{4}, \tag{33}$$

and slightly decreases $R_{\max}$:

$$R_{\max} = R_0 + (m_{\max} - 1)\delta. \tag{34}$$

The number of DFT bins per echo trip also increases:

$$\tilde{N} = \text{floor}\left(\frac{N}{m_{\max}}\right) = \text{floor}\left(\frac{\tilde{F}_p^0\lambda}{2\Delta v}\right). \tag{35}$$

Since $L_c$ is very large (on the order of $10^5$–$10^7$), the frequency spacing of the spurious, given by (27) with

$L_0$ replaced by $L_c$, is now greatly reduced. Thus, the number of spurious increases by a factor of $\Gamma$, with a corresponding reduction in average spurious power.

If the composite code is made sufficiently long so that the number of spurs is greater than or equal to the DFT length $N$, then the spurs merge in the spectrum and no longer appear discretely. If the composite code is too long ($L_c > N^2$), then perturbation of the phase code will be less than $2\pi$ over the entire DFT interval, which is too small to appreciably impact the spurious signals generated by the base phase code. Limiting the composite code length to $MN$ was found through simulation to yield a nearly uniform distribution of spurious power throughout the spectrum.

These considerations provide a lower and upper bound on the composite code length:

$$N \le L_c \le MN. \tag{36}$$

The DFT length should be selected to give an acceptable spectral resolution that is fine enough to resolve the spectrum of the narrowest expected cloud signal. This gives a minimum requirement for the DFT length and composite code length, by setting $\Delta v$ in (22) to $\sigma_v^{\min}$:

$$N_{\min} = \frac{M2v_a^0}{\sigma_v^{\min}} = \frac{MF_p^0\lambda}{2\sigma_v^{\min}}, \tag{37}$$

where $\sigma_v^{\min}$ is the signal's minimum expected velocity standard deviation in meters per second. For example, a Ka-band radar ($\lambda = 0.0086$), with a maximum range of 15 km ($F_p^0 = 10$ kHz), and range resolution of 15 m ($M = 500$), and assuming $\sigma_v^{\min} = 0.3\,\mathrm{m\,s^{-1}}$, should have a minimum DFT length and composite code length $N_{\min} = L_c^{\min} = 71\,666$. For this case, the maximum composite code length is $L_c^{\max} = 3.6 \times 10^7$.

When using a composite code, the average spurious power is given by

$$P_s^A = \frac{P_s^T}{N}, \tag{38}$$

since the total spurious power is distributed over all $N$ bins in the power spectrum. The average spurious power given by (38) limits the spectral dynamic range since the noise floor will be masked by the spurious power at high signal-to-noise ratio. An approximate formula for dynamic range when using a composite phase code as a function of the scattering volume spectral width is derived in appendix C.

## 6. Measurements in rain

A 10-W solid-state Ka-band radar operating at 35.68 GHz (Pazmany and Haimov 2018) was configured to gather QPC radar data in PMSW mode. The radar was modified for high duty cycle operation by increasing the capacity of the SSPA power supply and heat sink. Data were gathered with the antenna pointed into rain at a 45° elevation angle using a base code and composite code in quick succession:

1) Base code of length $M = 250$
2) Composite code of length 130 000 constructed with a base code of length $M = 250$

The pulse length at the T/R network antenna port was set to 150 ns and the pulse repetition interval (PRI) was 333.33 ns, yielding a duty cycle of 45% and range gate spacing of 50 m. The PRF multiplication factor of $M = 250$ resulted in a maximum unambiguous range of 12.5 km and maximum unambiguous velocity of 25.2 $\mathrm{m\,s^{-1}}$. A 65 000-point FFT was used to process both datasets, resulting in a velocity resolution $\Delta v$ of 0.194 $\mathrm{m\,s^{-1}}$, with $\tilde{N} = 260$ velocity bins per echo trip for the base code and $\tilde{N} = 261$ for the composite code. To reduce fluctuations in the power spectrum due to random fading, two successive 65 000-point power spectra were averaged to produce the final average power spectrum. The dwell time required to gather the 130 000 samples required to form the averaged power spectrum was 0.0433 s.

A range–Doppler plot for data gathered using the base code is presented in Fig. 7, generated from the average power spectrum with mean noise subtraction. The spectrum was sorted into successive Doppler spectra of length $\tilde{N}$ for each echo trip, and then the individual Doppler spectra were stacked to create the range–Doppler plot. For this dataset, range sidelobes due to amplitude and phase errors are clearly visible at an average level of −62 dB relative to the peak signal. The range sidelobe power corresponds to a combined phase and amplitude

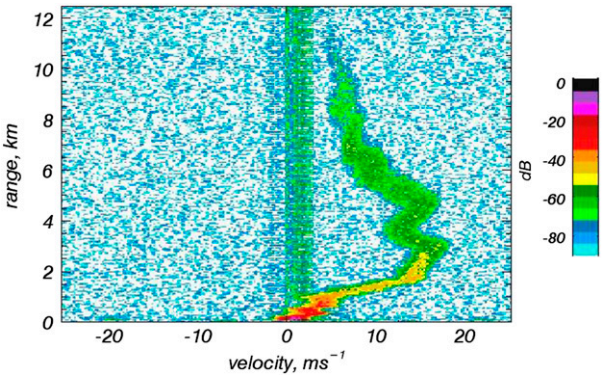


FIG. 7. Range–Doppler plot in rain with mean noise subtraction using a base code of length 250 and FFT length $N = 65\,000$ with two power spectra averaged for a total dwell time of 43.3 ms. Spurious-induced range sidelobes appear at all ranges with average peaks of 62 dB below the spectral peak of the maximum signal.

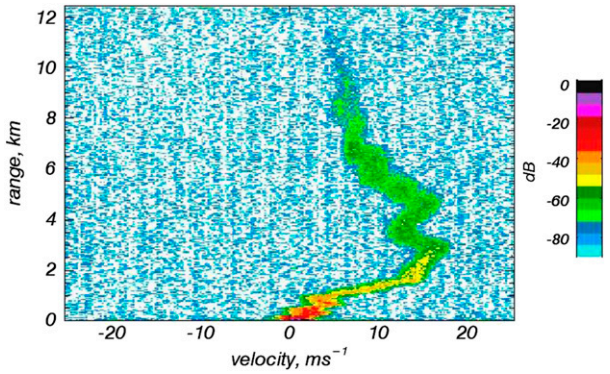


FIG. 8. Range–Doppler plot in rain with mean noise subtraction using a composite code of length 130 000 and FFT length $N$ = 65 000 with two power spectra averaged for a total dwell time of 43.3 ms. No spurious-induced range sidelobes are visible above the residual noise floor after mean noise subtraction.

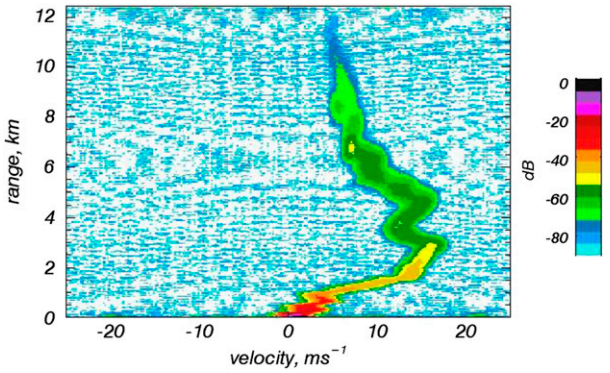


FIG. 9. Range–Doppler plot in rain with mean noise subtraction using a composite code of length 130 000 and FFT length $N$ = 65 000 with 90 power spectra averaged for a total dwell time of 1.95 s. The average spurious power is approximately 78 dB below the spectral peak of the maximum signal.

error standard deviation of $\sqrt{\sigma_\alpha^2 + \sigma_\varepsilon^2} = 0.012$, which was found from the ratio of total spurious power to the total signal power using (25).

The range–Doppler plot with mean noise subtraction for the case of the composite code is shown in Fig. 8. Since the spurious power is distributed over the entire power spectrum, it is no longer visible above the residual noise after mean noise subtraction. The spurious power becomes visible above the residual noise floor when averaging a large number of spectra. In Fig. 9, the number of spectra averaged was set to 90, for a total dwell time of 1.95 s. The spurious signals are visible throughout the spectrum, showing patterned clustering of the spurious power somewhat stronger than the residual noise floor. Assuming a combined phase and amplitude error standard deviation of 0.012 as was found with the base code, the theoretical average spurious level for the composite code given by (38) is −89 dB relative to the total signal power. The spectral dynamic range, as found using (C5) for the measured peak signal spectral width of 0.49 m s$^{-1}$ ($\sigma_n = 3.9 \times 10^{-5}$), is 78.1 dB.

QPC radar and conventional short-pulse data taken with a 6-s time delay between modes were gathered to demonstrate QPC radar signal processing gain. For this test, both modes employed a pulse length of 150 ns, with a maximum unambiguous range of 7.5 km (QPC radar: $F_p = 3$ MHz, $M = 150$; short-pulse PRI = 50 $\mu$s). The peak transmit power was 0.6 dB lower in QPC radar mode than in short-pulse mode, possibly because of a small drop in the SSPA power supply voltage when running at 45% duty cycle in QPC radar mode. The theoretical processing gain of QPC radar relative to short pulse with matching maximum range is equal to the PRF multiplication factor. Accounting for the small drop in transmit power, the expected processing gain of QPC radar with $M = 150$ is 10 log(150) − 0.6 dB or 21.1 dB. This is seen to agree with the measured data presented in Fig. 10, where SNR is plotted for short-pulse mode in the first 1 km overlaid by QPC radar mode SNR offset by the expected processing gain.

## 7. Summary and discussion

This paper has shown that quadratically varying phase codes applied to the transmit waveform on a pulse-by-pulse basis can be used to separate multiple echo trips in the spectral domain. This allows radar operation at very high pulse repetition frequencies, with a limiting case being PMSW mode where the transmit waveform is essentially a square wave with a single range gate sampling the received signal. The primary advantage of QPC radar as compared to conventional pulsed radar is the dramatic improvement in postprocessed SNR, which is proportional to the PRF

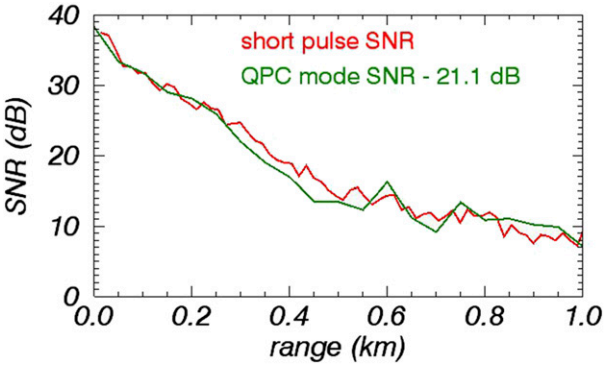


FIG. 10. Signal-to-noise ratio vs range in the first kilometer for short-pulse mode (red) and QPC radar mode (green) offset by 21.1 dB to account for the expected processing gain and 0.6-dB reduction in peak transmit power.

multiplication factor. QPC radar has two significant advantages over pulse compression radar. First, QPC radar has significantly lower range sidelobes when using composite phase codes than is usually achieved with pulse compression radar. Second, QPC radar's minimum range is identical to that of a conventional pulsed radar, determined only by the range resolution and the response time of the T/R network. The minimum range of a pulse compression radar typically much larger, being approximately equal to the pulse compression ratio times the range resolution.

The main requirements and limitations of QPC radar operation with a single-antenna system are summarized as follows:

1) The radar's transmitter must be capable of operating at 50% duty cycle to take full advantage of QPC radar operation.
2) High duty cycle operation in PMSW mode requires that the T/R network switching speed be a small fraction of the pulse width.
3) The received signal is undersampled in range, leading to gaps equal to the range resolution plus the T/R network response time between successive echo trips.
4) Range–Doppler ambiguity causes shifts in range when the magnitude of the velocity for a particular resolution volume exceeds $v_a^0$.
5) Phase and amplitude errors in the decoded waveform cause range sidelobes when using standard P3 codes, and limit dynamic range when using composite phase codes.

For dual-antenna operation at 100% duty cycle, no T/R network is required and there are no gaps in range. The PRF multiplication factor when operating at 100% duty cycle is given by

$$M = \frac{R_{\max}}{\Delta R_0}, \tag{39}$$

which is twice that of PMSW mode. When operating at 100% duty cycle, the analysis of range sidelobes and the effects of phase and amplitude errors are the same as in PMSW mode.

QPC radar operation allows radar systems to utilize most of an SSPA's available average power, which has heretofore only been practical in dual-antenna CW systems. When compared to a pulse compression radar beyond the minimum range of the pulse compression waveform, the improvement in postprocessed SNR for QPC radar will only be few decibels and may not justify the penalty of undersampling in range. However, at near ranges where pulse compression waveforms cannot be used, the improvement in postprocessed SNR of 20 dB or more when operating in QPC radar mode is substantial. Thus, QPC radar may be particularly useful in applications where near-range measurements are critical, such as in airborne cloud radars where comparison of radar data with data from wing-mounted in situ probes is of interest.

The ability of QPC radar to operate without serious range sidelobe contamination is useful when viewing weak signals in the presence of strong clutter. Pulse compression range sidelobes are a serious limitation for near-ground observations in airborne and spaceborne cloud and precipitation radars (McLinden et al. 2013). The absence of significant range sidelobes when using composite quadratic phase codes allows weakly scattering near-ground signals to be viewed without serious range sidelobe contamination. For measurements requiring low-range sidelobes in a single-antenna configuration QPC radar may be preferable to conventional pulse compression radars, provided range gaps can be tolerated.

In a dual-antenna system, the QPC radar technique can be implemented without T/R switching and can therefore operate at 100% duty cycle, eliminating gaps in the range profile inherent in single-antenna QPC radar operation. For dual-antenna systems employing conventional FMCW processing, the local oscillator used for deramping has a range-dependent offset from the received signal (Gurgel and Schlick 2009; Delanoë et al. 2016). This is typically handled by processing only a fraction of the available time domain signal with a corresponding loss in sensitivity and variable range resolution as a function of range (Delanoë et al. 2016; Küchler et al. 2017). In contrast, QPC radar processing yields uniform signal processing gain and constant range resolution at all sampled ranges from 0 to $R_{\max}$. This advantage suggests that QPC radar should be considered as an alternative to conventional FMCW radar in future dual-antenna systems.

*Acknowledgments.* The authors wish to thank their colleagues at ProSensing, Inc., for their work in developing the radar hardware and signal processing software used to demonstrate the QPC radar technique. We also wish to thank the reviewers, as well as D. Zrnic (NSSL) and S. Haimov (University of Wyoming), for their helpful suggestions.

## APPENDIX A

### Signal-to-Noise Ratio Optimization as a Function of Duty Cycle for PMSW Mode

The transmit waveform and receiver response are depicted in Fig. A1 for PMSW mode. The ideal pulse length $\tau_0$ is equal to one-half the pulse repetition interval, $T = 1/F_p$. The actual pulse length $\tau$ is foreshortened by the

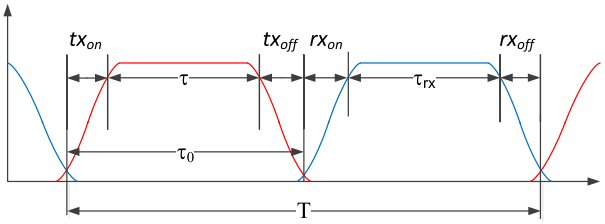


FIG. A1. Transmit waveform (red) and receiver response (blue).

transmitter response time, such that $\tau < \tau_0$. The receiver on-time $\tau_{rx}$ is equal to

$$\tau_{rx} = T - \tau - t_s,$$
$$t_s = tx_{\text{on}} + tx_{\text{off}} + rx_{\text{on}} + rx_{\text{off}}, \tag{A1}$$

where $t_s$ is the sum of the transmit and receiver response times. Let the pulse length $\tau$ vary as a function of duty cycle $D$; that is, $\tau = DT$. Assuming a rectangular transmit pulse, the matched filter is a rectangular filter of length $\tau$ and noise bandwidth $B = 1/\tau$. This is the optimal filter when $\tau \le \tau_{rx}$. When the receiver on time is less than the pulse length, the maximum possible filter length is $\tau_{rx}$ with bandwidth $\tilde{B} = \tau_{rx}^{-1}$, which is clearly suboptimal for a transmit pulse of length $\tau$. In other words, a matched filter cannot be implemented when $\tau > \tau_{rx}$. The optimal duty cycle occurs when $\tau = \tau_{rx}$ or

$$D_{\text{opt}} = \frac{T - t_s}{2T}. \tag{A2}$$

For example, $t_s \le 0.2T$ for the optimal duty cycle to exceed 40%, which results in signal processing gain that is within approximately 1 dB of the processing gain achieved with the theoretical optimal duty cycle of 50%.

## APPENDIX B

### Average Spurious Power due to Random Phase and Amplitude Errors

Consider the QPC radar architecture depicted in Fig. 1. The decoded signal samples $g(n)$ can be expressed as

$$g(n) = \sum_{m=0}^{M-1} e^{-j\phi_n} e^{j\phi_{n-m}} s_m(n), \tag{B1}$$

where the complex return signal voltage samples from the $m$th echo trip $s_m(n)$ is given by

$$s_m(n) = \int_0^{R_{\max}} p_f(m\delta - r) s(r, n)\, dr, \tag{B2}$$

where the transmitted pulse without phase coding and filtered by the receiver $p_f(r)$ is convolved with the scatterer distribution $s(r, n)$ and the echo trip spacing is given by $\delta = 0.5cF_p^{-1}$. From the definition of $\phi_n$ given by (3), the decoded signal is

$$g(n) = \sum_{m=0}^{M-1} e^{-j2\pi nm/M} e^{j\pi m^2/M} s_m(n). \tag{B3}$$

The phase term $e^{j\pi m^2/M}$ is only dependent on range, so it can be ignored.

Using an $N$-point DFT of the decoded signal samples, the frequency spectrum is obtained:

$$G(k) = \frac{1}{N} \sum_{n=0}^{N-1} g(n) e^{j2\pi nk/N}, \quad k = 0, 1, \ldots, N-1. \tag{B4}$$

Substituting (B3) for $g(n)$ gives

$$G(k) = \frac{1}{N} \sum_{m=0}^{M-1} \sum_{n=0}^{N-1} e^{-j2\pi nm/M} s_m(n) e^{j2\pi nk/N}, \tag{B5}$$

where the order of summation has been reversed. Let $S_m(k)$ be the spectral representation of $s_m(n)$:

$$S_m(k) = \frac{1}{N} \sum_{n=0}^{N-1} s_m(n) e^{j2\pi nk/N}. \tag{B6}$$

The first complex phase term in (B5) causes an $m$-dependent frequency shift of these spectral components. Therefore, (B5) can be written as

$$G(k) = \sum_{m=0}^{M-1} S_m\left(k + \frac{mN}{M}\right). \tag{B7}$$

Assume a random phase error, $\varepsilon = \varepsilon_n = f(\phi_n)$, and random amplitude error, $\alpha = \alpha_n = g(\phi_n)$, due to imperfections in the radar. These errors are periodic with period equal to the code length. Since the decoding is performed digitally, the decoding sequence is assumed to be ideal. The time domain signal after decoding is given by

$$g(n) = \sum_{m=0}^{M-1} e^{-j\phi_n} [e^{j(\phi_{n-m} + \varepsilon_{n-m})} + \alpha_{n-m}] s_m(n). \tag{B8}$$

For $\varepsilon \ll 1$, such that $\cos(\varepsilon) \approx 1$ and $\sin(\varepsilon) \approx \varepsilon$, $e^{j(\phi+\varepsilon)} \approx e^{j\phi}(1 + j\varepsilon)$, so

$$g(n) = \sum_{m=0}^{M-1} e^{-j\phi_n} (e^{j\phi_{n-m}} + \alpha_{n-m} + j\varepsilon_{n-m} e^{j\phi_{n-m}}) s_m(n), \tag{B9}$$

which can be separated into an ideal spectrum and error-induced spurious spectrum:

$$\tilde{G}(k) = G(k) + G_s(k) = G(k) + \frac{1}{N}\sum_{m=0}^{M-1}\sum_{n=0}^{N-1} e^{-j2\pi n^2/M}(\alpha_{n-m} + j\varepsilon_{n-m}e^{j\phi_{n-m}})s_m(n)e^{j2\pi nk/N} \quad \text{(B10)}$$

The spurious-induced term in (B10) due to phase and amplitude errors from a single echo trip $m$ expanded using (3) is

$$G_s(m,k) = \frac{1}{N}\sum_{n=0}^{N-1} e^{-j2\pi n^2/M}[\alpha_{n-m} + j\varepsilon_{n-m}e^{j2\pi(n-m)^2/M}] \times s_m(n)e^{j2\pi nk/N} \quad \text{(B11)}$$

Since $\alpha$ and $\varepsilon$ are zero mean, independent, and each term is uncorrelated from pulse to pulse, the expected average spurious power for the $m$th echo trip is

$$\langle|G_s(m,k)|^2\rangle = \frac{1}{N}(\langle\alpha^2\rangle + \langle\varepsilon^2\rangle)\langle|s_m|^2\rangle = \frac{1}{N}(\sigma_\alpha^2 + \sigma_\varepsilon^2)P_m, \quad \text{(B12)}$$

where $P_m$ is the average signal power from the $m$th echo trip. The total spurious power is the average spurious power summed over $N$ spectral bins:

$$P_s(m) = (\sigma_\alpha^2 + \sigma_\varepsilon^2)P_m. \quad \text{(B13)}$$

Summing over all echo trips gives the total spurious power in (25).

## APPENDIX C

### Spectral Dynamic Range when Using Composite Codes

When using a composite code, the spurious signals are distributed over all DFT bins if the composite code length meets the criteria given by (36). This implies that the level of the spurious limits the achievable dynamic range in the power spectrum. Assuming high SNR, so that the dynamic range is limited by the spurious power, the spectral dynamic range $D_s$, defined as the peak signal power divided by the average spurious power in (38), is given by

$$D_s = \frac{P_m^{\max}L_s}{P_s^A} \approx \frac{NP_m^{\max}L_s}{P_s^T}, \quad \text{(C1)}$$

where $P_m^{\max}$ is the average power in the range gate with the strongest signal return, $L_s$ is the signal spreading loss (Mead 2016), and the number of spurs is assumed to be approximately equal to the DFT length $N$ since the spectral region occupied by the signal is a small fraction of $N$. The signal spreading loss represents the reduction in peak power due to spectral broadening:

$$L_s = \text{erf}\left(\frac{1}{2\sqrt{2K_w^2 + 2N^2\sigma_n^2}}\right), \quad \text{(C2)}$$

where $K_W$ is a window-dependent scale factor ($K_W$ = 1.217 for a Hanning window) and the normalized spectral width is given by

$$\sigma_n = \frac{\sigma_v}{2v_a} = \frac{2\sigma_v}{F_p\lambda}, \quad \text{(C3)}$$

where $v_a$ is the unambiguous Doppler interval of the multiplied PRF and $\sigma_v$ is the full-width half-maximum spectral width in meters per second. For large $N$, ($N \gg K_w/\sigma_n$), spreading loss can be approximated by

$$L_s \approx \frac{1}{N\sigma_n}\sqrt{\frac{1}{2\pi}}, \quad \text{(C4)}$$

where the error function in (C2) is replaced by the first term of its Taylor series expansion. Therefore, for sufficiently long DFTs, the spectral dynamic range can be expressed as

$$D_s \approx \frac{P_m^{\max}}{P_s^T\sigma_n}\sqrt{\frac{1}{2\pi}} = \frac{P_m^{\max}}{(\sigma_\varepsilon^2 + \sigma_\alpha^2)\Sigma_P\sigma_n}\sqrt{\frac{1}{2\pi}}, \quad \text{(C5)}$$

which is accurate to within 1 dB for $N > 1.5K_w/\sigma_n$.

## REFERENCES


Barrick, D. E., 1973: FM/CW radar signals and digital processing. NOAA Tech. Rep. ERL 283-WPL 26, 22 pp., www.dtic.mil/dtic/tr/fulltext/u2/774829.pdf.

Chu, D., 1972: Polyphase codes with good periodic correlation properties. *IEEE Trans. Inf. Theory*, **18**, 531–532, https://doi.org/10.1109/TIT.1972.1054840.

Delanoë, J., and Coauthors, 2016: BASTA: A 95-GHz FMCW Doppler radar for cloud and fog studies. *J. Atmos. Oceanic Technol.*, **33**, 1023–1038, https://doi.org/10.1175/JTECH-D-15-0104.1.

Gurgel, K. W., and T. Schlick, 2009: Remarks on signal processing in HF radars using FMCW modulation. *Proc. Int. Radar Symp.*, Hamburg, Germany, German Institute of Navigation, 63–67.

Küchler, N., S. Kneifel, U. Löhnert, P. Kollias, H. Czekala, and T. Rose, 2017: A W-Band radar–radiometer system for accurate and continuous monitoring of clouds and precipitation. *J. Atmos. Oceanic Technol.*, **34**, 2375–2392, https://doi.org/10.1175/JTECH-D-17-0019.1.

Lee, R. W., 2015: Radar operation with increased Doppler capability. U.S. Patent 9057785, 37 pp.

Lewis, B. L., and F. F. Kretschmer Jr., 1982: Linear frequency modulation derived polyphase pulse compression codes. *IEEE Trans. Aerosp. Electron. Syst.*, **18**, 637–641, https://doi.org/10.1109/TAES.1982.309276.

——, ——, and W. W. Shelton, 1986: *Aspects of Radar Signal Processing*. Artech House, 554 pp.

Lundén, J., L. Terho, and V. Koivunen, 2005: Classifying pulse compression radar waveforms using time-frequency distributions. *2005 Conf. on Information Sciences and Systems*, Baltimore, MA, IEEE.

McLinden, M. L., J. Carswell, L. Li, G. Heymsfield, A. Emory, J. I. Cervantes, and L. Tian, 2013: Utilizing versatile transmission waveforms to mitigate pulse-compression range sidelobes with the HIWRAP radar. *IEEE Geosci. Remote Sens. Lett.*, **10**, 1365–1368, https://doi.org/10.1109/LGRS.2013.2241729.

Mead, J. B., 2016: Comparison of meteorological signal detectability with noncoherent and spectral-based processing. *J. Atmos. Oceanic Technol.*, **33**, 723–239, https://doi.org/10.1175/JTECH-D-14-00198.1.

Pazmany, A. L., and S. J. Haimov, 2018: Coherent power measurements with a compact airborne Ka-band precipitation radar. *J. Atmos. Oceanic Technol.*, **35**, 3–20, https://doi.org/10.1175/JTECH-D-17-0058.1.

Press, W. H., S. A. Teukolsky, W. T. Vetterling, and B. P. Flannery, 1988: *Numerical Recipes in C*. Cambridge University Press.

Raemer, H., 1996: *Radar Systems Principals*. CRC Press, 519 pp.

Sachidananda, M., and D. S. Zrnic, 1999: Systematic phase codes for resolving range overlaid signals in a Doppler weather radar. *J. Atmos. Oceanic Technol.*, **16**, 1351–1363, https://doi.org/10.1175/1520-0426(1999)016<1351:SPCFRR>2.0.CO;2.

Sirmans, D., and B. Bumgarner, 1975: Numerical comparison of five mean frequency estimators. *J. Appl. Meteor.*, **14**, 991–1003, https://doi.org/10.1175/1520-0450(1975)014<0991:NCOFMF>2.0.CO;2.

Skolnik, M. I., Ed., 1990: *Radar Handbook*. 2nd ed. McGraw-Hill, 1163 pp.

——, 2008: *Radar Handbook*. 3rd ed. McGraw-Hill, 1352 pp.